

Fabrication of quantum dot-immobilized Y_2O_3 microspheres with effective photoluminescence for cancer radioembolization therapy

Toshiki Miyazaki ^{a,b}, Takumi Wakayama^a, Masaru Oda^c and Masakazu Kawashita ^d

^aGraduate School of Life Science and Systems Engineering, Kyushu Institute of Technology, Kitakyushu, Japan;

^bCollaborative Research Center for Green Materials on Environmental Technology, Kyushu Institute of Technology, Kitakyushu, Japan;

^cGraduate School of Engineering, Kyushu Institute of Technology, Kitakyushu, Japan;

^dInstitute of Biomaterials and Bioengineering, Tokyo Medical and Dental University, Tokyo, Japan

ABSTRACT

Microspheres composed of Y-containing materials are effective agents for cancer radioembolization therapy using β -rays. The distribution and dynamics of these microspheres in tissues can be easily determined by providing the microspheres with an imaging function. In addition, the use of quantum dots will enable the detection of microspheres at the individual particle level with high sensitivity. In this study, core-shell quantum dots were bound to chemically modified yttria microspheres under various conditions, and the effect of reaction conditions on the photoluminescence properties of the microspheres was investigated. The quantum dots were immobilized on the surfaces of the microspheres through dehydration-condensation reactions between the carboxy groups of quantum dots and the amino groups of silane-treated microspheres. As the reaction time increased, the photoluminescence peak blue shifted, and the photoluminescence intensity and lifetime decreased. Therefore, a moderate period of the immobilization process was optimal for imparting effective photoluminescence properties. This study is expected to facilitate particle-level tracking of microsphere dynamics in biological tissues for the development of minimally invasive cancer radiotherapy of deep-seated tumors.

ARTICLE HISTORY

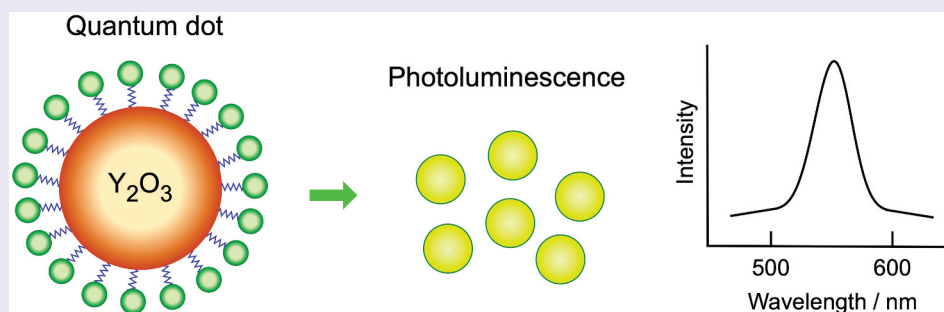
Received 20 December 2023

Revised 21 February 2024

Accepted 11 March 2024

KEYWORDS

Y_2O_3 microsphere; water-in-oil emulsion; quantum dot; chemical immobilization; photoluminescence; concentration quenching



IMPACT STATEMENT

We have established a method to immobilize quantum dots on yttria microspheres for cancer radiotherapy and revealed that photoluminescence intensity can be optimized by controlling the immobilization treatment time.

1. Introduction

Y-containing Materials are converted into β -ray emitters upon irradiation with neutrons. β -rays have a range of approximately 2.5 mm and cause little damage to surrounding normal tissues, making them suitable for cancer radiotherapy in deep-seated tumors [1,2]. In addition, microspheres composed of β -ray emitters with diameters of 20 to 30 μ m can be delivered through the capillaries of the

liver and kidney to embolize blood vessels near tumors, which cuts off the nutrient supply to tumors. This phenomenon is the basis of cancer radioembolization therapy using various Y-containing agents, such as Y_2O_3 -containing glass [2] and ^{90}Y -containing polymer microspheres [3]. The radioactivity is estimated to decay to negligible levels in 21 days because the half-life of ^{90}Y is 64.1 h [2]. In terms of biological safety, little cytotoxicity

CONTACT Toshiki Miyazaki  tmiya@life.kyutech.ac.jp  Graduate School of Life Science and Systems Engineering, Kyushu Institute of Technology, 2-4, Hibikino, Wakamatsu-ku, Kitakyushu 808-0196, Japan

 Supplemental data for this article can be accessed online at <https://doi.org/10.1080/14686996.2024.2331412>.

© 2024 The Author(s). Published by National Institute for Materials Science in partnership with Taylor & Francis Group.

This is an Open Access article distributed under the terms of the Creative Commons Attribution-NonCommercial License (<http://creativecommons.org/licenses/by-nc/4.0/>), which permits unrestricted non-commercial use, distribution, and reproduction in any medium, provided the original work is properly cited. The terms on which this article has been published allow the posting of the Accepted Manuscript in a repository by the author(s) or with their consent.

was observed in $Y_2O_3-Al_2O_3-SiO_2$ glass microspheres [4]. Although Y-containing microspheres themselves do not have cancer targeting ability, it is reported that those modified with magnetite particles exhibit a targeting function by a magnetic field [5]. Furthermore, Y_2O_3 nanoparticles are known to show selective cytotoxicity against cancer cells through the production of reactive oxygen species [6], making Y_2O_3 -based materials promising for cancer therapy from various perspectives.

Microspheres equipped with an imaging function can be monitored to determine their distribution and dynamics in tissues, thus ensuring that they do not migrate to healthy organs. Computed tomography, magnetic resonance imaging, and positron emission tomography have been used to observe the dynamics of ^{90}Y -containing microspheres [7–9], although they provide images of integrated microspheres. Therefore, observation of microspheres at the level of individual particles with high sensitivity is still challenging. In addition, observation of microspheres in thick tissue sections may be possible with laser-induced imaging. The thickness of the tissue section for optical microscopy generally needs to be several microns. As a light source, laser visible light (1 to 5 mm) penetrates deeper into biological tissues than normal visible light (<1 mm) [10,11].

Although quantum dots are attractive imaging agents because they can be detected with high sensitivity [12,13], they have not been conjugated to Y-containing microspheres. There are examples of quantum dots immobilized on $\gamma-Fe_2O_3$ nanoparticles and antibodies for biological applications [14,15]. In most cases, only one condition of the immobilization treatment is selected, and few studies have examined the effects of immobilization conditions on photoluminescence (PL) properties. In this study, core-shell quantum dots modified with carboxy groups were immobilized on amino group-modified Y_2O_3 microspheres through dehydration-condensation reactions under different conditions, and their PL properties were investigated. The material synthesis is schematically shown in Figure 1.

2. Materials and methods

2.1. Materials

Hydrogen peroxide (Nacalai Tesque, Kyoto, Japan), CdSe quantum dots (Sigma – Aldrich, St. Louis, MO), 3-aminopropyltriethoxysilane (APTES) (Shin-Etsu Chemical Co., Tokyo, Japan), 1-ethyl-3-(3-dimethylaminopropyl)carbodiimide hydrochloride (EDC·HCl) (Tokyo Chemical Industry Co., Tokyo, Japan), and other reagents (FUJIFILM Wako Pure Chemical Co., Osaka, Japan) were used without further purification.

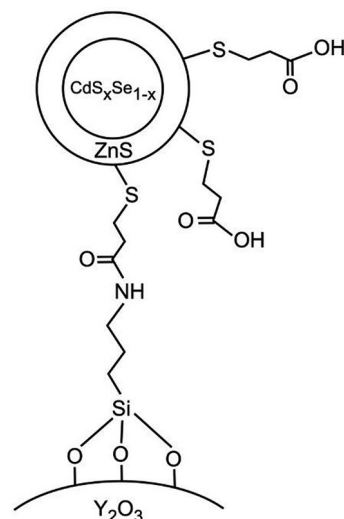


Figure 1. Schematic representation of the synthesis of CdSe quantum dot-immobilized Y_2O_3 microspheres.

2.2. Preparation of Y_2O_3 microspheres

Y_2O_3 microspheres were prepared using a previously published method [16]. A white precipitate was obtained by gradually dropping 25% NH_3 aqueous solution into 0.2 M $(CH_3COO)_3Y$ solution. The gel was then dehydrated using a centrifuge (CN-2060, AS ONE Co., Osaka, Japan) and washed with ultra-pure water. Then, 15 mL of 0.1 M HNO_3 was added to the gel, and the mixture was stirred at room temperature for 24 h to prepare a yttrium hydroxide sol. Next, 10 mL of the sol, as the aqueous phase, and 50 mL of kerosene with 0.1 mass% of sorbitan monooleate, as the oil phase, were mixed and stirred for 10 min at different speeds using a homogenizer (Homogenizing Mixer Mark II, PRIMIX Co., Hyogo, Japan). Then, 150 mL of 1-butanol as the dehydrating agent was quickly added to the obtained water-in-oil emulsion, and the mixture was stirred for 10 min. The reaction product was then filtered, washed with acetone, and dried at 60°C. The powder sample was then placed in an alumina crucible and then into an electric furnace (KDF-300Plus, Denken – Highdental Co., Kyoto, Japan), and the temperature was raised to 1100°C at a rate of 5°C/min. The sample was calcined at this temperature for 2 h.

2.3. Chemical modification of microspheres

The obtained microspheres (400 mg) were immersed in a mixture of 50% H_2SO_4 and 30% hydrogen peroxide solution (10 mL, volume ratio = 3:1) and shaken at the speed of 90 strokes/min for 20 min in a water bath (Personal H-10, TAITEC Co., Saitama, Japan) at room temperature. The purpose of this treatment was to remove organic matter from the surface and to increase the surface coverage of hydroxyl groups to improve the efficiency of the following silane coupling

treatment. The samples were then filtered and dried at 60°C. APTES was dissolved in 90% ethanol aqueous solution at various concentrations up to 0.5 M. The treated microspheres (100 mg) were immersed in 50 mL of the APTES solution and shaken at the rate of 140 strokes/min for 1 h at room temperature. After the APTES treatment, the samples were filtered, dried at 60°C for 1 h, and finally heat-treated at 120°C for 30 min.

APTES-treated microspheres (50 mg) were added to a mixture of borate buffer (10 mL, pH 7.3), CdS_xSe_{1-x}/ZnS core-shell quantum dots modified with 3-mercaptopropionic acid (0.1 mL, 1 mg/mL) [17], EDC-HCl (2 mmol), and N-hydroxysuccinimide (2 mmol). The mixture was shaken at the rate of 120 strokes/min at room temperature. The samples were then filtered, washed with borate buffer and ultrapure water, and dried at 60°C. Crystalline structure and light-absorption properties of the used quantum dots were shown in supplementary information.

2.4. Characterization

The microstructure of the samples was characterized using scanning electron microscopy (SEM, S-3500N, Hitachi, Tokyo, Japan), Fourier-transform infrared spectroscopy (FT-IR, FT/IR-6100, JASCO, Tokyo, Japan), X-ray photoelectron spectroscopy (XPS, KRATOS, Shimadzu, Kyoto, Japan) and field emission transmission electron microscope (FE-TEM, JEM-F200, JEOL Ltd., Tokyo, Japan). For SEM, the surfaces of the samples were coated with a Au/Pd thin film by ion sputtering (E-101, Hitachi). For FT-IR, the milled samples were mixed with KBr powder at the mass ratio of 1:60. The powder mixture was pressed to form a thin film for measurements. For FE-TEM, samples were supported on a copper mesh coated with triacetylcellulose and carbon and acceleration voltage was fixed at 200kV. The surface charge of the samples in 10 mM NaCl solution was measured using a zeta-potential analyzer (ELS-Z, Otsuka Electronics Co., Osaka, Japan). The amount of amino groups on the sample surface was determined using the ninhydrin reaction. Namely, the microspheres were reacted with the ninhydrin reagent, and the change in absorbance at 570 nm was examined using ultraviolet-visible (UV-vis) spectrophotometry (V-630, JASCO).

2.5. Optical measurements

We used an inverted optical microscope (TE-2000 U, Nikon, Tokyo, Japan) equipped with a 10X objective (NA = 0.4) and a 2D charge-coupled device (CCD) detector (Cascade-512B, Teledyne Photometrics, Tucson, AZ) to take reflection and PL images of the quantum dot-immobilized Y₂O₃ particles cast on silica glass substrates with a thickness of 1 mm. The samples

were illuminated with white light from a tungsten-halogen lamp to acquire reflection images. PL images were acquired in the configuration of total internal reflection fluorescence microscopy (TIRFM). A solid-state laser (Sapphire 488-50, Coherent, Santa Clara, CA) with a wavelength of 488 nm was used as the excitation source.

To acquire PL spectra and decay curves, a pulsed diode laser (LDH-PC405, PicoQuant, Berlin, Germany) with a wavelength of 407.5 nm was used to excite the quantum dot-immobilized sample (10 mg) placed in a transparent glass bottle. A multi-channel spectrometer (SpectraPro-300i, Acton Research Co., Acton, MA) equipped with liquid nitrogen-cooled CCD (LN/CCD, Princeton Instruments, Trenton, NJ) was used to obtain PL spectra. A streak camera (C4334, Hamamatsu Photonics K.K., Shizuoka, Japan) was used to measure PL decay curves. The measured curves were fitted to the sum of two exponential decay functions: $A_1 \exp(-t/\tau_1) + A_2 \exp(-t/\tau_2)$, where τ_1 and τ_2 are the fluorescence lifetime of each component and A_1 and A_2 are constants representing the mixing ratio of each component. The average lifetime was calculated as $A_1\tau_1 + A_2\tau_2$ from each decay curve.

3. Results

According to the X-ray diffraction patterns, the calcined particles were composed of a single phase of cubic Y₂O₃. Figure 2 shows the SEM micrographs of the surfaces of particles prepared at different emulsification speeds. Most of the obtained particles were spherical, and some of the particles resembled fused spheres. The particle size slightly decreased as the rotation speed increased. From the images ($n = 300$), the average particle sizes of the particles prepared at 2000, 2500, and 3000 rpm were 22.1 ± 9.9 , 18.7 ± 7.4 , and 14.9 ± 5.3 μm, respectively. Although the microspheres prepared at 3000 rpm were slightly smaller than the ideal size for cancer embolization therapy, their coefficient of variation (standard deviation per average particle size) was the smallest. Therefore, the particles prepared at 3000 rpm were used in subsequent surface treatments.

As shown in Figure 3, the amino group content of the Y₂O₃ microspheres increased as the APTES concentration increased and remained almost constant when the APTES concentration was above 0.4 M. Figure 4 shows FE-TEM photograph the surface of Y₂O₃ microsphere after treatment with the quantum dot-containing solution for 6 h. Particles with diameter around 5 nm were distributed near the top surface. Figure 5 shows the XPS spectra of the surfaces of the Y₂O₃ microspheres before and after the treatment with the quantum dot-containing solution for 24 h. The spectrum of the untreated

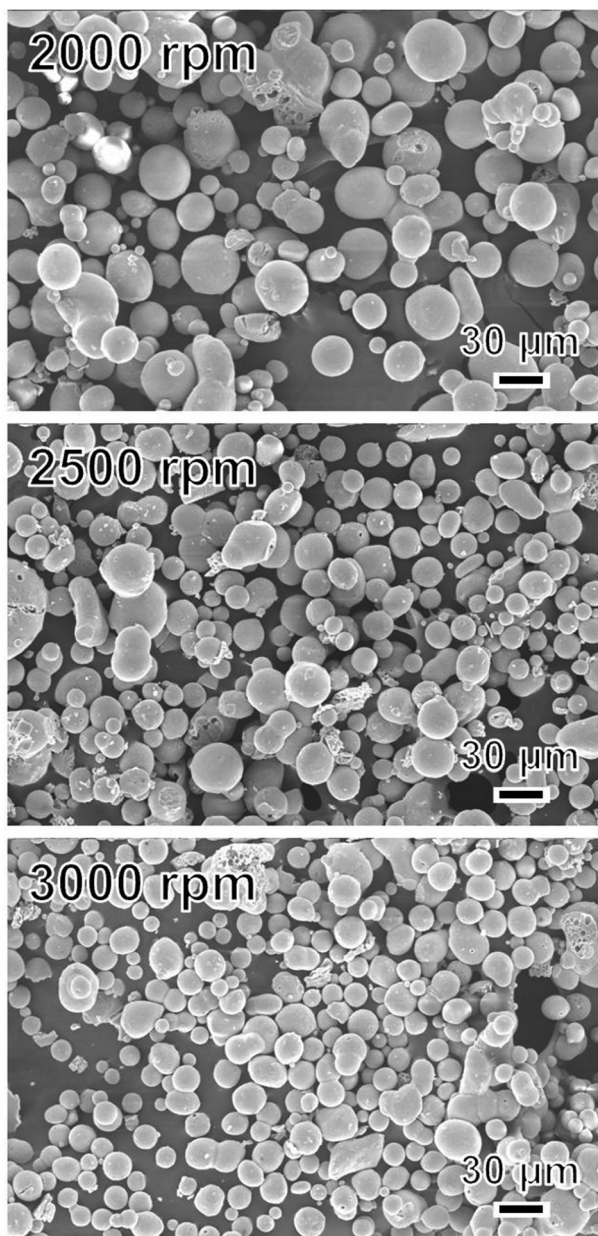


Figure 2. SEM micrographs of the surfaces of particles prepared at different emulsification speeds.

microspheres contained a N1s peak derived from APTES and Y3s peak derived from the microspheres, while the spectrum of the treated microspheres contained these peaks and an additional Cd3s peak derived from quantum dots, indicating that CdSe quantum dots were immobilized on the microsphere surface. In addition, the position of the N1s peak slightly shifted to a higher binding energy after the treatment. The binding energy of the amide group is approximately 1 eV higher than that of the amino group [18]. Therefore, this shift indicated that amide bonds were constructed through dehydration – condensation reactions during the treatment. As shown in Figure 6, the FT-IR spectra of samples treated for more than 3 h contained peaks at 1600 and 1700 cm^{-1} , which were assigned to the amide groups.

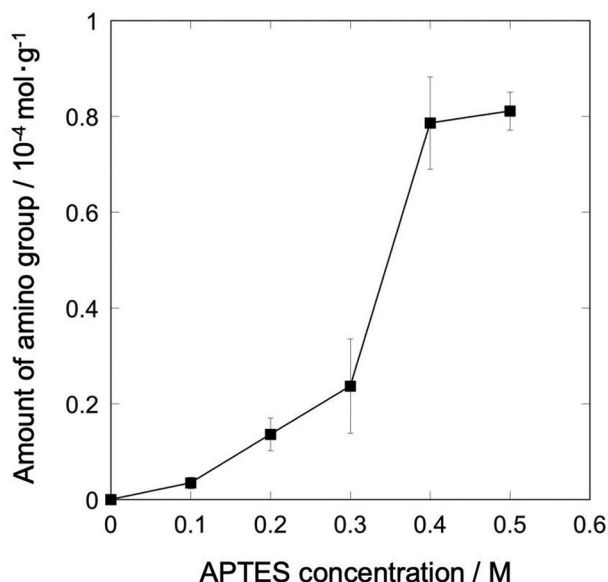


Figure 3. Amino group content of Y_2O_3 microspheres as a function of APTES concentration.

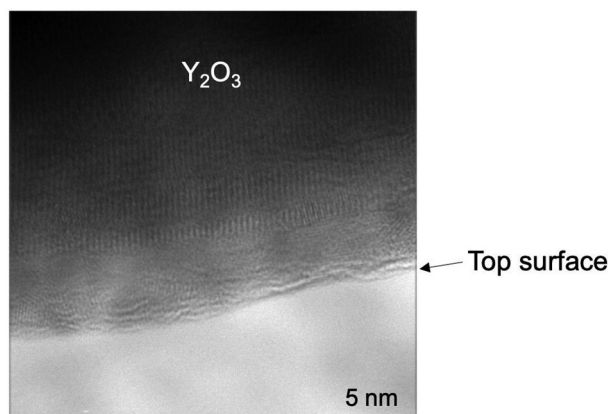


Figure 4. FE-TEM photograph the surface of Y_2O_3 microsphere after treatment with the quantum dot-containing solution for 6 h.

Figure 7 shows the zeta potential of the samples treated with the quantum dot-containing solution for various periods. The zeta potential was approximately 30 mV before the treatment but was negative and hovered between -10 and -20 mV after the treatment.

Figure 8 shows the reflection and PL images of the microspheres treated with the quantum dot-containing solution for 3 h. Some of the microspheres in the reflection image showed luminescence. Figure 9 shows the PL spectra of the microspheres treated with the quantum dot-containing solution for various periods along with the PL spectrum of the quantum dot solution as received. The bare quantum dots showed luminescence at approximately 550 nm, which blue shifted after they were immobilized on the microspheres. Compared with the fluorescence intensity of the bare quantum dots, the fluorescence intensity of the immobilized quantum dots decreased slightly at the treatment time of 6 h and further decreased to less

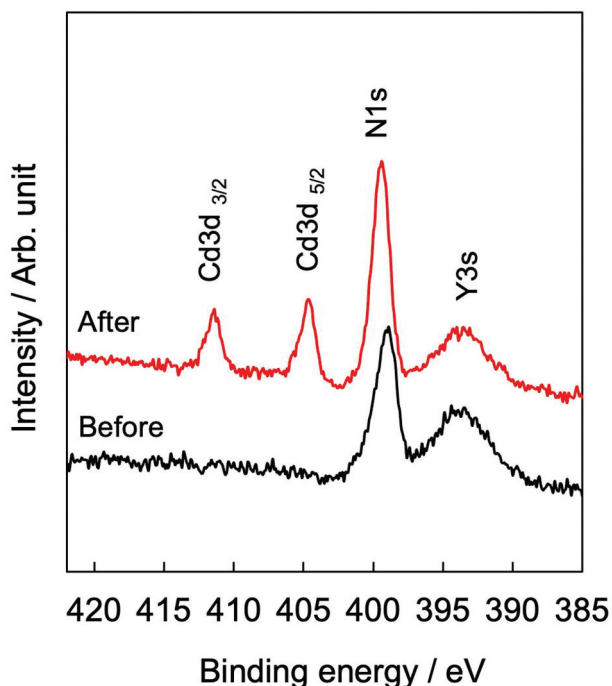


Figure 5. XPS spectra of the surfaces of Y_2O_3 microspheres before and after treatment with the quantum dot-containing solution for 24 h.

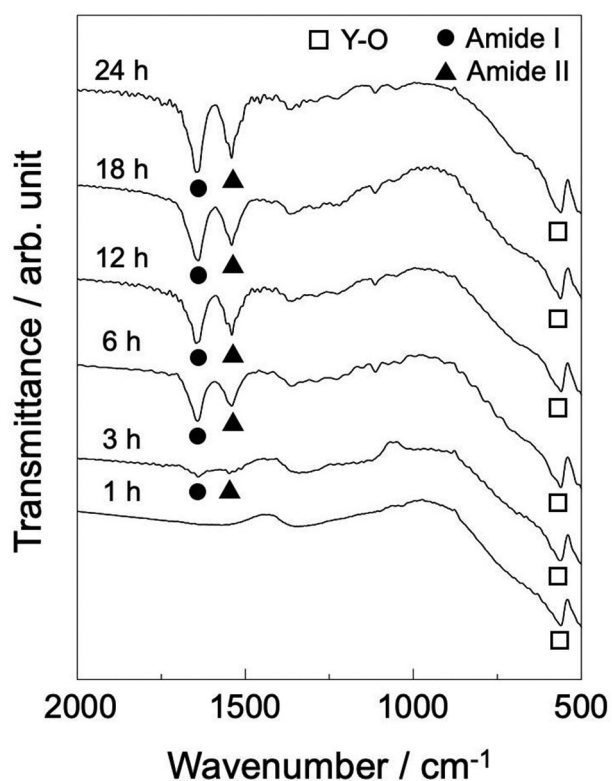


Figure 6. FT-IR spectra of the surfaces of Y_2O_3 microspheres treated with the quantum dot-containing solution for various periods.

than half as the treatment time increased to 12 h or longer. The PL decay curves of the samples (Figure 10) showed that the degree of attenuation increased in the order: 6 h < Solution < 3 h < 12 h < 24 h < 18 h. In addition,

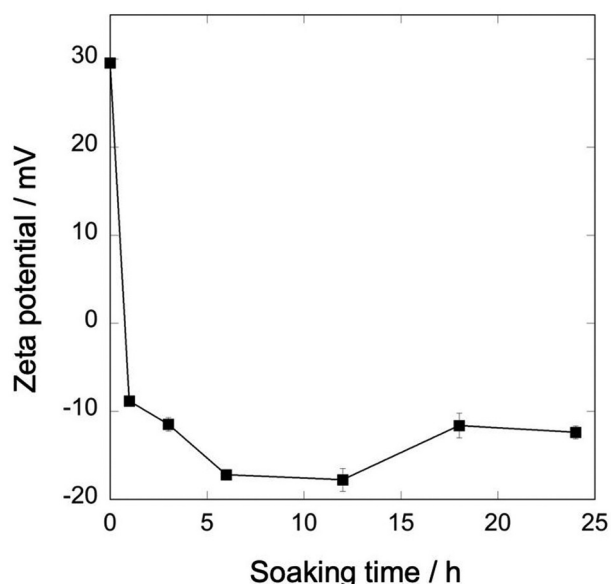


Figure 7. Zeta potential of samples treated with the quantum dot-containing solution for various periods.

the PL lifetimes (Table 1), obtained by curve fitting the decay curves, showed the same tendency as the degree of attenuation.

4. Discussion

Y_2O_3 microspheres were obtained by dehydrating water-in-oil emulsions. The particles became smaller as the rotation speed increased owing to the increased shear force of the homogenizer, which was consistent with the trend previously reported [16]. Some particles appeared to merge into fused spheres, which likely occurred because of the buoyancy arising from the density difference between the Y_2O_3 (density of approximately 5 g/cm^3) and kerosene (specific gravity of 0.78 to 0.80). In the future, the use of a heavier oil phase may suppress the fusion of microspheres and reduce the size variation.

The quantum dots were chemically immobilized on the surface of Y_2O_3 microspheres via amino groups (Figure 1), which was supported by FE-TEM (Figure 4), XPS (Figure 5), and FT-IR (Figure 6) results. Judging from the absorption intensity of the amide groups in FT-IR, the amount of the immobilized quantum dot may increase with treatment time.

The amount of immobilized amino groups did not change significantly as the APTES concentration increased beyond 0.4 M (Figure 3). The amount of hydroxyl groups on Y_2O_3 microspheres before the APTES treatment, measured using the zinc complex substitution method [19], was $1.33 \times 10^{-4} \text{ mol}\cdot\text{g}^{-1}$. Consequently, APTES was bound to approximately 60% of the surface hydroxyl groups at the APTES concentration of 0.4 M. Immobilization of additional APTES molecules is likely suppressed by the steric hindrance of immobilized APTES molecules.

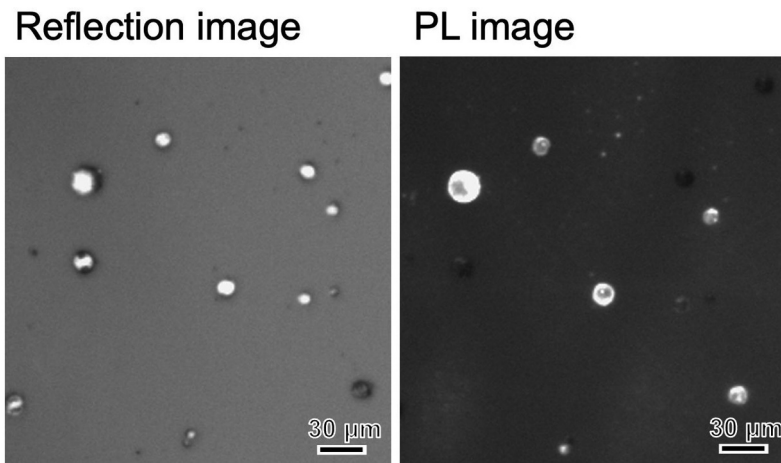


Figure 8. Reflection and PL images of microspheres treated with the quantum dot-containing solution for 3 h.

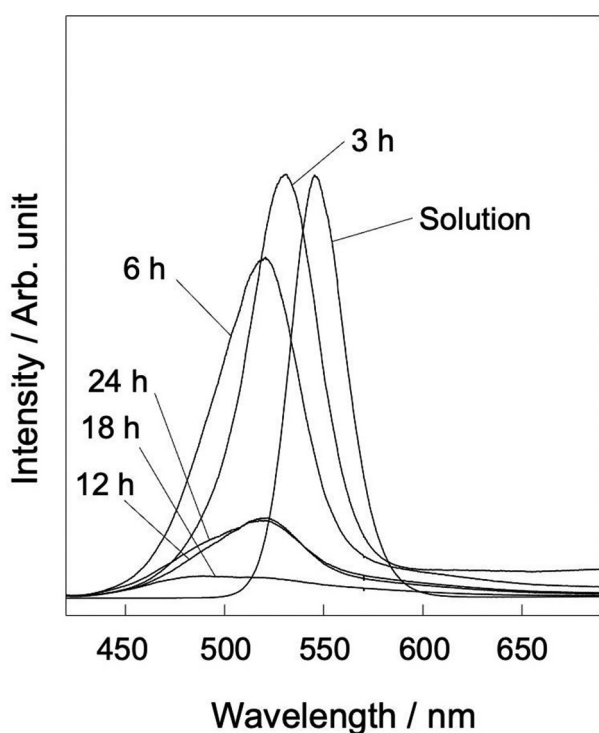


Figure 9. PL spectra of the quantum dot solution as received and microspheres treated with the quantum dot-containing solution for various periods.

Initially, we expected PL to enhance without a change in the lifetime if we increased the treatment time for the immobilization of quantum dots. However, the obtained results revealed that the PL intensity and lifetime decreased as the treatment

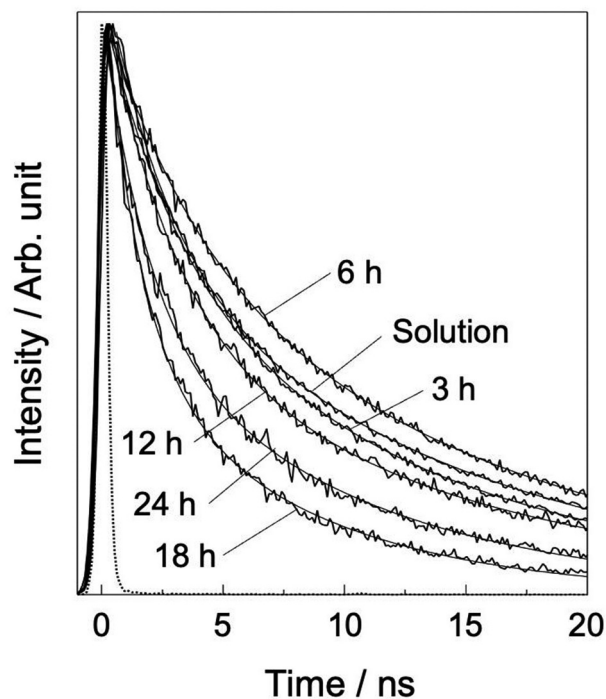


Figure 10. Decay curves of the quantum dot solution as received and microspheres treated with the quantum dot-containing solution for various periods. Dotted lines represent instrument response function, while smooth solid lines indicate fitting curves.

time increased (Figures 9 and 10, Table 1). Therefore, the treatment time should be limited to 6 h or less to prevent quenching from the aggregation of quantum dots. It has been reported that

Table 1. Photoluminescence decay times of the quantum dot solution as received and microspheres treated with the quantum dot-containing solution for various periods. Values were calculated by fitting the decay curves.

Sample	A ₁	τ ₁ /ns	A ₂	τ ₂ /ns	Decay time/ns
Solution	0.63	14	0.48	2.5	10
3 h	0.57	13	0.42	3.2	8.9
6 h	0.65	15	0.38	3.8	11
12 h	0.48	14	0.58	3.0	8.4
18 h	0.44	7.6	0.63	1.5	4.3
24 h	0.50	9.6	0.53	1.8	5.8

a small amount of hydroxyl groups is present on the ZnS surface, which constitutes the shell of the quantum dots [20]. These hydroxyl groups form ester bonds with the carboxy groups on other quantum dots through dehydration – condensation reactions, resulting in stacks of quantum dots on the Y_2O_3 microspheres. The surface zeta potentials of all quantum dot-treated samples were below -10 mV (Figure 7), indicating that there was no correlation between the surface potential and PL properties. However, the zeta potential reflects only the topmost surface of the materials, and thus it does not change with stacking. Fluorescence quenching from the aggregation of quantum dots has been reported [18,19]. The sample treated for 24 h showed higher PL intensity than that treated for 18 h (Figure 9). Since there was almost no change in zeta potential and absorption intensity of amide groups in FT-IR, it seems that the amount of quantum dot immobilization is not remarkably different. However, judging from the FE-TEM result showing the aggregation of the quantum dots, there may be a difference in the aggregation state between the above samples.

The PL spectra blue shifted when the treatment time for quantum dot immobilization increased (Figure 9), indicating that the PL wavelength can be controlled by adjusting the treatment condition. The PL wavelength is often red-shifted when quenching occurs through the aggregation of quantum dots [21,22]. Blue shifting of the emission wavelength has been reported to occur through the immobilization of polar molecules [23]. This effect may be responsible for the blue shift observed in the present study because the relative permittivity of Y_2O_3 is approximately 12, which is directly proportional to the dipole moment, an indicator of molecular polarity [24]. The PL of quantum dots immobilized on various solid surfaces has been studied, although there is no unified trend in terms of the direction of the peak shift. For example, quantum dots immobilized on γ - Fe_2O_3 nanoparticles exhibit blue-shifted PL [14], while CdSe quantum dots integrated with ferroelectric $BaTiO_3$ exhibit red-shifted PL [25]. Because there are other factors governing the emission-wavelength shift, such as compressive stress [26] and the Stark effect induced by charged molecules [27], further investigations are required to elucidate the cause of the shift in detail.

The results of this study indicate that there are optimum conditions for the immobilization of quantum dots on solid surfaces through dehydration – condensation reactions. This information is expected to facilitate the effective immobilization of quantum dots on various functional solids, including biomaterials.

5. Conclusions

Quantum dots were immobilized on Y_2O_3 microspheres to impart PL properties. The microsphere surface was modified with amino groups by silane coupling to facilitate the immobilization of CdSe quantum dots through subsequent dehydration – condensation reactions. A moderate period of the immobilization process was optimal for imparting effective PL properties. This study is expected to contribute to the development of minimally invasive cancer radiotherapy of deep-seated tumors by facilitating particle-level tracking of microsphere dynamics in biological tissues. Furthermore, if the primary particle size of Y_2O_3 constituting the microspheres can be controlled by synthetic conditions, it is expected to provide the microspheres with selective anti-cancer functions.

Acknowledgments

We acknowledge Mr. Noboru Wakayama, Center for Instrumental Analysis, Kyushu Institute of Technology, for FE-TEM observation. We also thank Edanz (<https://jp.edanz.com/ac>) for editing a draft of this manuscript.

Disclosure statement

No potential conflict of interest was reported by the author(s).

ORCID

Toshiki Miyazaki  <http://orcid.org/0000-0001-5642-0096>
Masakazu Kawashita  <http://orcid.org/0000-0002-4329-9001>

References

- [1] Kawashita M. Ceramic microspheres for biomedical applications. *Int J Appl Ceram Tech.* 2005;2(3):173–183. doi: [10.1111/j.1744-7402.2005.02023.x](https://doi.org/10.1111/j.1744-7402.2005.02023.x)
- [2] Day DE, Day TE. Radiotherapy glasses. In: Hench L, editor. *An introduction to bioceramics*. 2nd ed. London: Imperial College Press; 2013. p. 431–446.
- [3] Campbell AM, Bailey IH, Burton MA. Analysis of the distribution of intra-arterial microspheres in human liver following hepatic yttrium-90 microsphere therapy. *Phys Med Biol.* 2000;45(4):1023–1033. doi: [10.1088/0031-9155/45/4/316](https://doi.org/10.1088/0031-9155/45/4/316)
- [4] Radu T, Chiriac MT, Popescu O, et al. *In vitro* evaluation of the effects of yttria–alumina–silica microspheres on human keratinocyte cells. *J Biomed Mater Res A.* 2013;101A(2):472–477. doi: [10.1002/jbm.a.34320](https://doi.org/10.1002/jbm.a.34320)
- [5] Häfeli UO, Sweeney SM, Beresford BA, et al. Magnetically directed poly(lactic acid) ^{90}Y -microspheres: novel agents for targeted intracavitary radiotherapy. *J Biomed Mater Res.* 1994;28(8):901–908. doi: [10.1002/jbm.820280809](https://doi.org/10.1002/jbm.820280809)
- [6] Emad B, WalyEldeen AA, Hassan H, et al. Yttrium oxide nanoparticles induce cytotoxicity, genotoxicity,

- apoptosis, and ferroptosis in the human triple-negative breast cancer MDA-MB-231 cells. *BMC Cancer*. 2023;23(1):1151. doi: [10.1186/s12885-023-11649-w](https://doi.org/10.1186/s12885-023-11649-w)
- [7] Lewandowski RJ, Thurston KG, Goin JE, et al. ^{90}Y microsphere (TheraSphere) treatment for unresectable colorectal cancer metastases of the liver: response to treatment at targeted doses of 135–150 Gy as measured by ^{18}F fluorodeoxyglucose positron emission tomography and computed tomographic imaging. *J Vasc Interv Radiol*. 2005;16(12):1641–1651. doi: [10.1097/01.RVI.0000179815.44868.66](https://doi.org/10.1097/01.RVI.0000179815.44868.66)
- [8] Kamel IR, Reyes DK, Liapi E, et al. Functional MR imaging assessment of tumor response after ^{90}Y microsphere treatment in patients with unresectable hepatocellular carcinoma. *J Vasc Interv Radiol*. 2007;18(1):49–56. doi: [10.1016/j.jvir.2006.10.005](https://doi.org/10.1016/j.jvir.2006.10.005)
- [9] Flamen P, Vanderlinden B, Delatte P, et al. Multimodality imaging can predict the metabolic response of unresectable colorectal liver metastases to radioembolization therapy with yttrium-90 labeled resin microspheres. *Phys Med Biol*. 2008;53(22):6591–6603. doi: [10.1088/0031-9155/53/22/019](https://doi.org/10.1088/0031-9155/53/22/019)
- [10] Ash C, Dubec M, Donne K, et al. Effect of wavelength and beam width on penetration in light-tissue interaction using computational methods. *Lasers Med Sci*. 2017;32(8):1909–1918. doi: [10.1007/s10103-017-2317-4](https://doi.org/10.1007/s10103-017-2317-4)
- [11] Finlayson L, Barnard IRM, McMillan L, et al. Depth penetration of light into skin as a function of wavelength from 200 to 1000 nm. *Photochem Photobiol*. 2022;98(4):974–981. doi: [10.1111/php.13550](https://doi.org/10.1111/php.13550)
- [12] Smith AM, Gao X, Nie S. Quantum dot nanocrystals for in vivo molecular and cellular imaging. *Photochem Photobiol*. 2004;80(3):377–385. doi: [10.1562/0031-8655\(2004\)080<0377:QDNFIV>2.0.CO;2](https://doi.org/10.1562/0031-8655(2004)080<0377:QDNFIV>2.0.CO;2)
- [13] Courty S, Luccardini C, Bellaiche Y, et al. Tracking individual kinesin motors in living cells using single quantum-dot imaging. *Nano Lett*. 2006;6(7):1491–1495. doi: [10.1021/nl060921t](https://doi.org/10.1021/nl060921t)
- [14] Wang D, He J, Rosenzweig N, et al. Superparamagnetic Fe_2O_3 Beads–CdSe/ZnS quantum dots core–shell nanocomposite particles for cell separation. *Nano Lett*. 2004;4(3):409–413. doi: [10.1021/nl035010n](https://doi.org/10.1021/nl035010n)
- [15] Torchynska TV, Casas Espinola JL, Díaz Cano A, et al. Emission of CdSe/ZnS and CdSeTe/ZnS quantum dots conjugated to IgG antibodies. *Physica E*. 2013;51:60–64. doi: [10.1016/j.physe.2013.03.023](https://doi.org/10.1016/j.physe.2013.03.023)
- [16] Miyazaki T, Kai T, Ishida E, et al. Fabrication of yttria microcapsules for radiotherapy from water/oil emulsion. *J Ceram Soc Japan*. 2010;118(6):479–482.
- [17] Xie R, Kolb U, Li J, et al. Synthesis and characterization of highly luminescent CdSe-core CdS/Zn_{0.5}Cd_{0.5}S/ZnS multishell nanocrystals. *J Am Chem Soc*. 2005;127(20):7480–7488.
- [18] Graf N, Yegen E, Gross T, et al. XPS and NEXAFS studies of aliphatic and aromatic amine species on functionalized surfaces. *Surf Sci*. 2009;603(18):2849–2860. doi: [10.1016/j.susc.2009.07.029](https://doi.org/10.1016/j.susc.2009.07.029)
- [19] Sakamoto H, Hirohashi Y, Saito H, et al. T. Effect of active hydroxyl groups on the interfacial bond strength of titanium with segmented polyurethane through γ -mercapto propyl trimethoxysilane. *Dent Mater J*. 2008;27(1):81–92.
- [20] Dengo N, Vittadini A, Natile MM, et al. In-depth study of ZnS nanoparticle surface properties with a combined experimental and theoretical approach. *J Phys Chem*. 2020;124(14):7777–7789. doi: [10.1021/acs.jpcc.9b11323](https://doi.org/10.1021/acs.jpcc.9b11323)
- [21] Noh M, Kim TH, Lee H, et al. Fluorescence quenching caused by aggregation of water-soluble CdSe quantum dots. *Colloids Surf A*. 2010;359(1–3):39–44. doi: [10.1016/j.colsurfa.2010.01.059](https://doi.org/10.1016/j.colsurfa.2010.01.059)
- [22] Wu M, Mukherjee P, Lamont DN, et al. Electron transfer and fluorescence quenching of nanoparticle assemblies. *J Phys Chem C*. 2010;114(13):5751–5759. doi: [10.1021/jp9098667](https://doi.org/10.1021/jp9098667)
- [23] Borkovska LV, Korsunska NE, Kryshtab TG, et al. Effect of conjugation with biomolecules on photoluminescence and structural characteristics of CdSe/ZnS quantum dots. *Semiconductors*. 2009;43(6):775–781. doi: [10.1134/S1063782609060177](https://doi.org/10.1134/S1063782609060177)
- [24] Jatar S. Relationship between dielectric constant of liquids and solids and dipole moments. *Nature*. 1944;153(3877):222. doi: [10.1038/153222a0](https://doi.org/10.1038/153222a0)
- [25] Zhou J, Li L, Gui Z, et al. Photoluminescence of CdSe nanocrystallites embedded in BaTiO₃ matrix. *Appl Phys Lett*. 2000;76(12):1540–1542. doi: [10.1063/1.126089](https://doi.org/10.1063/1.126089)
- [26] Meulenberg RW, Jennings T, Strouse GF. Compressive and tensile stress in colloidal CdSe semiconductor quantum dots. *Phys Rev B*. 2004;70(23):235311. doi: [10.1103/PhysRevB.70.235311](https://doi.org/10.1103/PhysRevB.70.235311)
- [27] Empedocles SA, Bawendi MG. Quantum-confined stark effect in single CdSe nanocrystallite quantum dots. *Science*. 1997;278(5346):2114–2117. doi: [10.1126/science.278.5346.2114](https://doi.org/10.1126/science.278.5346.2114)